Adaptive Control of Haptic Interaction with Impedance and Admittance Type Virtual Environments

Amin Abdossalami Shahin Sirouspour*

ABSTRACT

Adaptive nonlinear controllers have been proposed to improve the stability and transparency in haptic rendering. Through a separation of control and dynamic simulation, the proposed controllers can couple impedance-type haptic devices with impedance and admittance-type virtual environment simulators. The intervening dynamics of the interface, subject to stability constraints, can be replaced with an adjustable mass-damper tool within the proposed framework. Nonlinear dynamics for haptic device and parametric uncertainty in user's arm dynamics are considered in the design of controllers which require position, velocity and force measurements. The transparency and stability of the proposed haptic control systems are investigated using a Lyapunov analysis. The controllers are implemented on a two-axis impedance-type haptic device for interacting with impedance and admittance-type virtual environments. In the impedance-type environment, interaction with a virtual wall is modeled by a spring-damper coupler. This model along with an alternative constraint-based rigid wall model are employed in the admittance-type simulations. Although the two controllers behave similarly in free motion, the controller for admittance-type environments is capable of rendering markedly stiffer rigid contacts.

Index Terms: Haptics, Haptic Interaction, Adaptive Control, Transparency, Rigid Contact, Virtual Environment.

1 INTRODUCTION

Rendering of perceptual reality through machine made force feedback, haptics, is finding growing applications in teleoperation, virtual reality training simulators, computer-aided virtual prototyping, and gaming. Haptic rendering algorithms are employed either to provide direct interaction with virtual environments or to produce virtual fixtures in robot manipulating tasks. The ultimate goal of haptics is to break the boundaries between reality and virtuality and to achieve maximum transparency, i.e. solid constraints should feel sufficiently rigid in contact and no hindering effects must be felt in free motion.

Due to the increasing sophistication of virtual environment simulators, haptic systems have evolved from using integrated algorithms for dynamic simulation and control to separating them into two independent processes. Within such a framework, the role of control routine is to provide an interconnection between the dynamic simulation and the haptic interface [7]. For instance in the case of an impedance-type device and an admittance-type virtual environment, the controller is usually a spring-damper virtual coupler [23]. In this case, although the environment constraint can be infinitely stiff, the maximum impedance presented to the user in rigid contact is limited by the stability constraints arising from the discrete-time implementation of the controller. Inherent delay and data loss due to sample-and-hold, limited control update rate, sensor quantization and encoder resolution, actuator dynamics and inherent dynamics of haptic device are the main factors affecting the stability and fidelity of haptic interaction. They ultimately limit the range of the impedance (Z-width) [5] that can be displayed to the user. The reader is referred to [1, 8] for a review of these effects.

Control of haptic interfaces has been an active field of research in recent years. In [6] a passivity-based approach was employed to derive relationships between intrinsic damping of haptic device and the maximum gains in virtual coupler controller to guarantee closed-loop stability. In [2] the two-port network theory was used to analyze the stability of haptic control systems. The concept of passivity observer (PO) and passivity controller (PC) was introduced in [14] for guaranteeing the stability of haptic interaction. It was shown in [9] that inherent resistor-inductor of the motor can be utilized in a voltage drive analog circuit to achieve higher stiffness than traditional approaches. A time-domain passivity control scheme was utilized in [13] by applying tunable hardware dissipation. There is an inherent asymmetry in human manipulation and force perception [16]. While one may be incapable of moving his/her fingertip at frequencies higher than 10Hz, human fingertips can perceive stimulus in a frequency range of dc to 1kHz, with the highest sensitivity around 250Hz [3]. This motivated the works of [11, 19] in which combinations of closed-loop and transient open-loop force generation have been proposed to provide more realistic rendering of rigid contacts.

There are two major classes of controllers for force feedback in virtual environments, i.e. impedance-type control [15] and admittance-type control [10]. Impedance-type controllers use the displacement of haptic end-effector, and sometimes the operator's applied force to control the force applied to the haptic device. Admittance-type controllers, on other hand, use the operator's applied force, and sometimes the additional input of the end effector displacement to control the position of haptic device. Some reports on the classification and analysis of haptic control schemes are given in [4, 12, 21] but no discussion of closed-loop stability is provided in these papers. Similarly, there are impedance and admittance classes of robotic manipulators. Impedance-type robots, including most of the existing haptic devices, are characterized by their low inertia and high backdrivability and are usually controlled by impedance-type controllers. They are more suited for the rendering of free motion and soft contact interactions. The admittance-type robots, however, are mostly characterized by their high inertia, low backdrivability and are usually controlled with admittance-type controllers. In the context of haptics, these devices have good performance in rendering rigid contacts but are at disadvantage in free motion and soft contacts [10].

In many applications, specially those with high force output requirements, the actual dynamics of an impedance-type device may be significant enough to interfere with the user's perception of the virtual environment in free motion and contact. In addition, simple virtual coupler controllers are often incapable of properly rendering rigid contacts. To address these issues, novel adaptive nonlinear controllers are proposed here that can improve the stability and performance of haptic interaction with impedance haptic devices. In-

*S. Sirouspour is with the Department of Electrical and Computer Engineering, McMaster University, Hamilton, Ontario, Canada. e-mail: sirouspour@ece.mcmaster.ca

Symposium on Haptic Interfaces for Virtual Environments and Teleoperator Systems 2008
13-14 March, Reno, Nevada, USA
978-1-4244-2005-6/08/$25.00 ©2008 IEEE

teraction with both impedance and admittance-type virtual environment simulations are considered. The proposed controllers, which require hand force measurement in addition to postion/velocity, are compatible with the nonlinear dynamics of the haptic device and can adapt to variations in the user and device dynamics. They can replace the actual dynamics of the haptic interface with that of a mass-damper tool with adjustable parameters. Using a Lyapunov analysis, the stability and performance of the proposed controllers for interacting with admittance and impedance-type environments are analyzed.

The rest of this paper is organized as follows. In Section 2 mathematical models of the haptic control system are provided. In Section 3, the proposed haptic rendering controllers are introduced. Closed-loop stability of the haptic interaction under the proposed control laws is investigated in Section 4. Experimental results are given in Section 5. Finally, the paper is concluded in Section 6.

2 HAPTIC DEVICE DYNAMICS

The dynamics of a haptic device in workspace coordinates can be written as

$$M_{Robot}(x)\ddot{x} + C_{Robot}(x,\dot{x})\dot{x} + F_{dRobot}\dot{x} + G_{Robot}(x) = f_{Human} + f_u \quad (1)$$

where x, $\dot{x}$, $\ddot{x} \in \Re^n$ represent the device workspace position, velocity and acceleration vectors, $M_{Robot}(x) \in \Re^{n\times n}$ is the device inertia matrix, $C_{Robot}(x,\dot{x}) \in \Re^{n\times n}$ represents centripetal and Coriolis effects, $F_{dRobot} > 0$ contains damping coefficients, $G_{Robot}(x) \in \Re^n$ is a vector of gravitational force, $f_u \in \Re^n$ denotes the control input force, and $f_{Human} \in \Re^n$ is the user hand force. The hand force may be modeled using a linear passive mass-spring-damper impedance and an exogenous force input, i.e. [18]

$$f_{Human} = f^*_{Human} - M_{Hand}\ddot{x} - F_{dHand}\dot{x} - K_{Hand}x \quad (2)$$

where $M_{Hand} \in \Re^{n\times n}$, $F_{dHand} \in \Re^{n\times n}$, $K_{Hand} \in \Re^{n\times n}$, are constant inertia, damping, and stiffness matrices, respectively. The term $f^*_{Human} \in \Re^n$ is the human exogenous force input which passes through the hand dynamics (2) to produce sensor measurement hand force f_{Human}. The dynamics of the haptic device in (1) and the user in (2) can be combined as follows

$$M(x)\ddot{x} + C(x,\dot{x})\dot{x} + F_d\dot{x} + G(x) = f^*_{Human} + f_u \quad (3)$$

$$\begin{aligned} M(x) &= M_{Robot}(x) + M_{Hand} \\ C(x,\dot{x}) &= C_{Robot}(x,\dot{x}) \\ F_d &= F_{dRobot} + F_{dHand} \\ G(x) &= G_{Robot}(x) + K_{Hand}x \end{aligned}$$

The following properties of (3) are later used in this paper [17].

Property I : The inertia matrix $M(x)$ is symmetric and uniformly poitive-definite $\forall x \in \Re^n$, satisfying the following inequalities

$$m_1\|\zeta\|^2 \le \zeta^T M(x)\zeta \le m_2\|\zeta\|^2 \qquad \forall\zeta \in \Re^n \quad (4)$$

where $\|.\|$ is standard Euclidean norm and m_1 and m_2 are known positive constants.

Property II : For a particular choice of $C(x,\dot{x})$ the following skew-symmetry property holds

$$\zeta^T(\frac{1}{2}\dot{M}(x) - C(x,\dot{x}))\zeta = 0 \qquad \forall\zeta \in \Re^n \quad (5)$$

Property III : The dynamic model described in (3) can be linearly parameterized in terms of a vector of unknown parameters $\theta \in \Re^p$ as follows

$$M(x)\ddot{x}_r + C(x,\dot{x})\dot{x}_r + F_d\dot{x}_r + G(x) - f^*_{Human} = \Upsilon_r(x,\dot{x},\dot{x}_r,\ddot{x}_r)\theta \quad (6)$$

where $\Upsilon_r(x,\dot{x},\dot{x}_r,\ddot{x}_r) \in \Re^{n\times p}$ is a dynamic regression matrix, $\dot{x}_r$ and $\ddot{x}_r$ are the reference signals that will be introduced later in the paper.

Property IV : The norm of $C(x,\dot{x})$ is upper bounded as follows

$$\|C(x,\dot{x}))\| \le \eta\|\dot{x}\| \quad (7)$$

where η is a positive constant.

3 ADAPTIVE CONTROL OF HAPTIC INTERFACES

The adaptive controllers proposed here are based on the Slotine's passivity-based position controller [20] and the adaptive motion/force controller in [22]. In the first step, the goal is to derive the control input and parameter estimation laws so that the device velocity $\dot{x}(t)$ tracks a reference signal $\dot{x}_r(t)$ to be defined later. To this end, the control signal in (3) is chosen as

$$f_u = \Upsilon_r(x,\dot{x},\dot{x}_r,\ddot{x}_r)\hat{\theta} - K_d s \quad (8)$$

where

$$s = \dot{x} - \dot{x}_r \quad (9)$$

and $\hat{\theta}$ is an estimate of the unknown parameters, $K_d > 0$ is constant, and Υ_r has been defined in (6).

By substituting the control input from (8) into the system dynamics in (3) one may obtain

$$M(x)\dot{s} + C(x,\dot{x})s + (F_d + K_d)s = \Upsilon_r(x,\dot{x},\dot{x}_r,\ddot{x}_r)\tilde{\theta} \quad (10)$$

where $\tilde{\theta} = \hat{\theta} - \theta$.

It should be noted that the user exogenous input force f^*_{Human} has been treated as an unknown system parameter and has been included in the parameter vector θ. As it will be seen shortly, the parameter adaptation law is derived based on the assumption that the unknown parameters are constant which is obviously invalid in the case of f^*_{Human}. However, if the adaptation is much faster than the rate of change in f^*_{Human}, such approximation may still be used. Alternatively, given a priori known bound on f^*_{Human}, a switching term such as $-k\text{sgn}(s)$ can be employed to suppress this disturbance [18]. However, such an approach would generate excessive chattering in the control system and may even cause instability by exciting unmodeled dynamics.

3.1 Admittance-type Virtual Environments

The structure of the haptic control system for interacting with admittance-type virtual environments in shown in Fig. 1. In this case, the environment force f_e is the input to the dynamic simulation, and the environment acceleration $\ddot{x}_e$, velocity $\dot{x}_e$ and position x_e are calculated based on this input force. A virtual intervening mass-damper tool must be integrated into the dynamic simulation to avoid an ill-conditioned solution in free motion. To facilitate the subsequent stability analysis, it is assumed here that the resulting acceleration $\ddot{x}_e$ of the tool/environmnet is bounded. This can be simply achieved by limiting this quantity at the simulation output to an arbitrarily large value without affecting the system response. The reference signal $\dot{x}_r$ in (8) is defined as

$$\dot{x}_r = \dot{x}_e - \Lambda(x - x_e) \quad (11)$$

where $\Lambda = \Lambda^T > 0$. It can be concluded from (9) that

$$s = \dot{x} - \dot{x}_e + \Lambda(x - x_e) \quad (12)$$

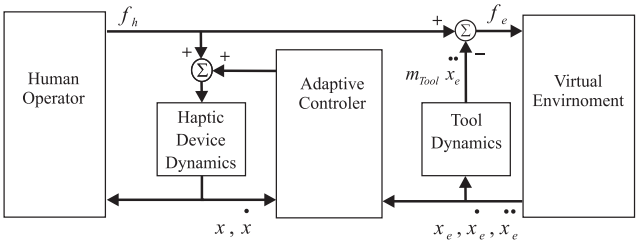

Figure 1: Adaptive control for interacting with admittance-type VE.

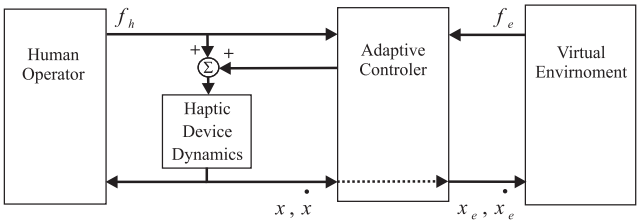

Figure 2: Adaptive control for interacting with impedance-type VE.

Equation (12) represents a stable first-order dynamic system in terms of $\tilde{x} = x - x_e$ with the term s as its input. The haptic device control problem can now be formulated as the regulation of the variable s to zero in which case the haptic device position and velocity would converge to those of the tool/environment. Therefore, the user would feel the virtual environment through the adjustable tool dynamics that replace the inherent dynamics of the haptic device. It should be noted that the implementation of this controller requires the measurement of x, $\dot{x}$, and f_h. Although the position and the force can be directly measured by sensors, the device velocity may be approximated by numerical differentiation and filtering of the position signal.

3.2 Impedance-type Virtual Environments

The structure of the haptic control system for interacting with impedance-type virtual environments is displayed in Fig. 2. In this case, the haptic device position x and velocity $\dot{x}$ are passed to the virtual environment simulation as x_e and $\dot{x}_e$. In response, the simulation returns the reaction force f_e generated based on the environment model which can be a simple spring-damper. It should be noted that impedance-type environments would require acceleration of the haptic device for rendering inertial forces and as such are more suitable for simulation of spring-damper forms of contact.

In this case the reference signal $\dot{x}_r$ in (8) is defined as

$$\dot{x}_r = A(\bar{f}_h - \bar{f}_e) + (1-\beta)\dot{\tilde{x}} \tag{13}$$

where $A, \beta > 0$ are constants, $\bar{f}_h$, $\bar{f}_e$, $\dot{\tilde{x}}$ are filtered versions of f_h, f_e, $\dot{x}$, respectively. These filters are given by (also see Fig.3)

$$\dot{\bar{f}}_h = C(f_h - \bar{f}_h) \tag{14}$$

$$\ddot{\tilde{x}} = C(\dot{x} - \dot{\tilde{x}}) \tag{15}$$

Substituting $\dot{x}_r$ from (13) into (9) yields

$$\bar{f}_h - \bar{f}_e = (AC)^{-1}\ddot{\tilde{x}} + A^{-1}\beta\dot{\tilde{x}} - A^{-1}s \tag{16}$$

which implies that, provided $s \to 0$ and the bandwidth of the first-order filters C is sufficiently high, the user would interact with the virtual environment through a mass-damper tool with a mass of $(AC)^{-1}kg$ and a damping of $(A^{-1}\beta)\frac{N.s}{m}$ which are adjustable through the parameters A, C, and β. In other words, the haptic device inherent dynamics are replaced by this synthesized tool. It should be noted that the control signal in (8) requires $\ddot{x}_r$. It is easy to see that the special form of $\dot{x}_r$ in (13) eliminates the need for the measurement of $\ddot{x}$, $\dot{f}_h$ and $\dot{f}_e$ in the control implementation.

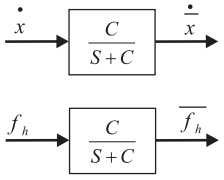

Figure 3: First-order filters are used in the definition of the reference signal in case of impedance-type VE.

4 Stability Analysis

In this section It will be shown that:

Stability: Employing the control action (8) in (3) results in a stable closed-loop system, i.e. x, $\dot{x}$ and $\hat{\theta}$ are bounded.

Performance: The tracking error term $s \in L_2 \cap L_\infty$ and also converges to zero.

To this end, the following nonnegative function is defined as a candidate Lyapunov function

$$V = \frac{1}{2}s^T M(x)s + \frac{1}{2}\tilde{\theta}^T\Gamma^{-1}\tilde{\theta} \quad \geq 0 \tag{17}$$

where $\Gamma = \Gamma^T > 0$ is constant. By taking the derivative of (17) along the closed-loop state trajectory in (10)[1]

$$\dot{V} = s^T(\Upsilon_r\tilde{\theta} - C(x,\dot{x})s - F_d s - K_d s) + \frac{1}{2}s^T\dot{M}(x)s + \tilde{\theta}^T\Gamma^{-1}\dot{\tilde{\theta}} \tag{18}$$

The following element-wise adaptation law for the vector of unknown parameters is proposed

$$\dot{\hat{\theta}}_k = \begin{cases} 0, & \hat{\theta}_k \leq (\hat{\theta}_{min})_k \quad and \quad (\Upsilon_r^T s)_k \geq 0 \\ 0, & \hat{\theta}_k \geq (\hat{\theta}_{max})_k \quad and \quad (\Upsilon_r^T s)_k \leq 0 \\ -(\Gamma\Upsilon_r^T s)_k, & \text{otherwise.} \end{cases} \tag{19}$$

where k represents the k^{th} vector element. The vectors $\hat{\theta}_{min}$ and $\hat{\theta}_{max}$ contain the minimum and maximum allowable values for the parameters respectively. By employing (5) and (19) in (18), one can write

$$\dot{V} \leq -s^T(F_d + K_d)s \quad \leq 0 \tag{20}$$

The inequality in (20) is a direct consequence of F_d and K_d being positive definite. One can conclude from (20) and (17) that s and $\tilde{\theta}$, and hence $\hat{\theta}$ are all bounded. Also, from (20) it is evident that $s \in L_2$ and therefore, $s \in L_2 \cap L_\infty$.

In the case of interaction with an impedance-type virtual environment, (16) can be used to derive

$$\bar{f}_h^* = \left(M_{Hand} + M_e + (AC)^{-1}\right)\ddot{\tilde{x}} + \left(F_{dHand} + B_e + A^{-1}\beta\right)\dot{\tilde{x}} + (K_{Hand} + K_e)\bar{x} - A^{-1}s \tag{21}$$

where linear mass-spring-damper models have been used for the user and the virtual environment. M_e, B_e, and K_e, are the environment constant inertia, damping, and stiffness matrices, respectively.

[1]For brevity $\Upsilon_r(x, \dot{x}, \dot{x}_r, \ddot{x}_r)$ is replaced with Υ_r

Given that $\bar{f}_h^*$ can be assumed bounded, $\ddot{\bar{x}}$, $\dot{\bar{x}}$, and $\bar{x}$ are bounded and thus $\dot{x}$ and x are both bounded. Note that if the stiffness values of the hand K_{Hand} and the environment K_e are both zero, only the boundedness of $\dot{x}$ can be concluded. Now from the boundedness of $\dot{x}$ and (10), it can be shown that $\dot{s}$ is bounded and hence using the Barbalat's Lemma [20], it can be concluded that $s \rightarrow 0$.

For haptic interaction with admittance-type virtual environments, using $s \in L_2 \cap L_\infty$, the Lemma 1 in [22], and (12) one may show that

$$\dot{\tilde{x}}, \tilde{x} \in L_2 \cap L_\infty \tag{22}$$

Using (22), linear mass-spring-damper models for the user and environment, and the following from Fig.1

$$f_h = (M_e + m_{Tool})\ddot{x}_e + B_e\dot{x}_e + K_e x_e \tag{23}$$

it can be easily shown that

$$x,\ \dot{x} \in L_\infty \tag{24}$$

Now using the assumption on boundedness of the environment acceleration output $\ddot{x}_e$, it can be demonstrated that

$$\dot{x}_r, \ddot{x}_r \in L_\infty \tag{25}$$

and thus the application of the Barbalat's lemma would result in s converging to zero.

By taking the integral of both sides in (20) and knowing that the Lyapunov function V is non-increasing, it can be shown that

$$\int_0^\infty \|s(\tau)\|^2 d\tau \leq \frac{1}{\sigma_{\min}(F_d + K_d)}(V(0) - V(\infty)) \Rightarrow$$
$$\|s\|_2^2 \leq \frac{1}{2\sigma_{\min}(F_d + K_d)}\left(m_2\|s(0)\|^2 + \sigma_{\max}(\Gamma^{-1})\|\widetilde{\theta}(0)\|^2\right) \tag{26}$$

where $\sigma_{\min}(.)$ and $\sigma_{\max}(.)$ denote the minimum and maximum singular values for the corresponding matrices respectively. The upper bound on the L_2 norm of the transient error s in (26) is a function of initial errors $s(0)$ and $\widetilde{\theta}(0)$ as well as the control and adaptation gains. Increasing the adaptation gain Γ and the feedback gain K_d would improve the performance of the system by reducing the upper bound on $\|s\|_2^2$. However in practice, these gains are limited by the presence of measurement noise that can excite high frequency unmodeled dynamics and potentially cause instability. Finally, it must be pointed out that the proposed continuous-time control framework allows for synthesizing an arbitrary intervening virtual tool mass in interaction with both impedance and admittance-type environments. Nevertheless, the minimum achievable tool mass is limited in a discrete-time implementation of the controllers due to stability constraints arising from computation delay and zero-order-hold effect. The impact of a discrete-time implementation on the stability of the proposed controllers will be studied in future.

5 Experimental Results

The Quanser pantograph device shown in Fig. 4 is employed to evaluate the proposed controllers. This device has two active axes of motion in the horizontal x-y plane and is actuated by the direct-drive DC motors attached to its proximal links. The motor shaft angles are measured by optical encoders with 20,000 counts per revolution. A Mini40 force/torque sensor from the ATI Industrial Automation has been mounted on haptic device end-effector to measure the hand force f_{Human}. The control code runs under Matlab RTW/Tornado VxWorks real-time operating system with a sampling frequency of 2048 Hz.

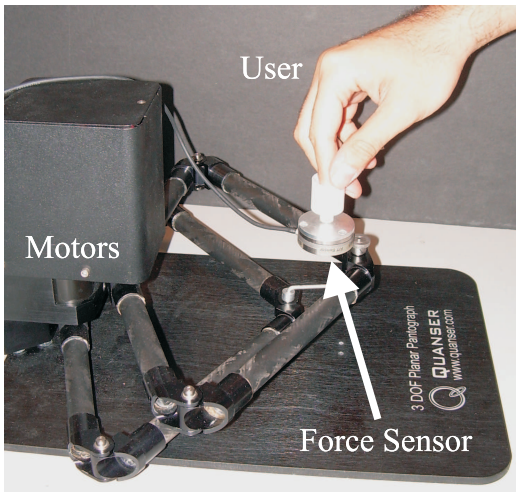

Figure 4: Experimental setup.

Table 1: Design and Simulation Parameters

Parameter	Value
m_{Tool}	$0.35kg$
K_d	10
Λ	100
C	400 $\frac{rad}{s}$
β	0
A	0.01
k_{wall} For case 1, impedance-type wall	4000 $\frac{N}{m}$
k_{wall} For case 1, admittance-type wall	10000 $\frac{N}{m}$
k_{wall} For Impedance-type VE	1000 $\frac{N}{m}$
b_{wall} For case 1, impedance-type wall	40 $\frac{N.s}{m}$
b_{wall} For case 1, admittance-type wall	300 $\frac{N.s}{m}$
b_{wall} For Impedance-type VE	20 $\frac{N.s}{m}$
Γ_{11}	200
Γ_{22}	1400
Γ_{33}	4000
M_1	0.5 kg
M_2	0.5 kg
k_1 and k_2	1000 $\frac{N}{m}$
b_1 and b_2	3 $\frac{N.s}{m}$
Sampling Rate	2048 Hz

Three admittance-type and one impedance-type haptic simulations have been implemented and their results are reported here. The dynamic simulation and control parameters are given in Table 1.

5.1 Admittance-type Virtual Environment Simulation

In this case, the hand force f_{Human} is measured by the force sensor along the x and y axes in the horizontal plane and is passed to the dynamic simulation. A virtual tool in the form of a mass $m_{Tool} = 0.35kg$ has also been implemented. The value of the mass has been selected to maintain the closed-loop stability in the discrete-time implementation of the controller. Matlab's Euler integration routine has been used to simulate the environment dynamics.

5.1.1 Free Motion

In free motion, the environment force is zero and the user would only feel the dynamics of the virtual tool which replace those of the device.

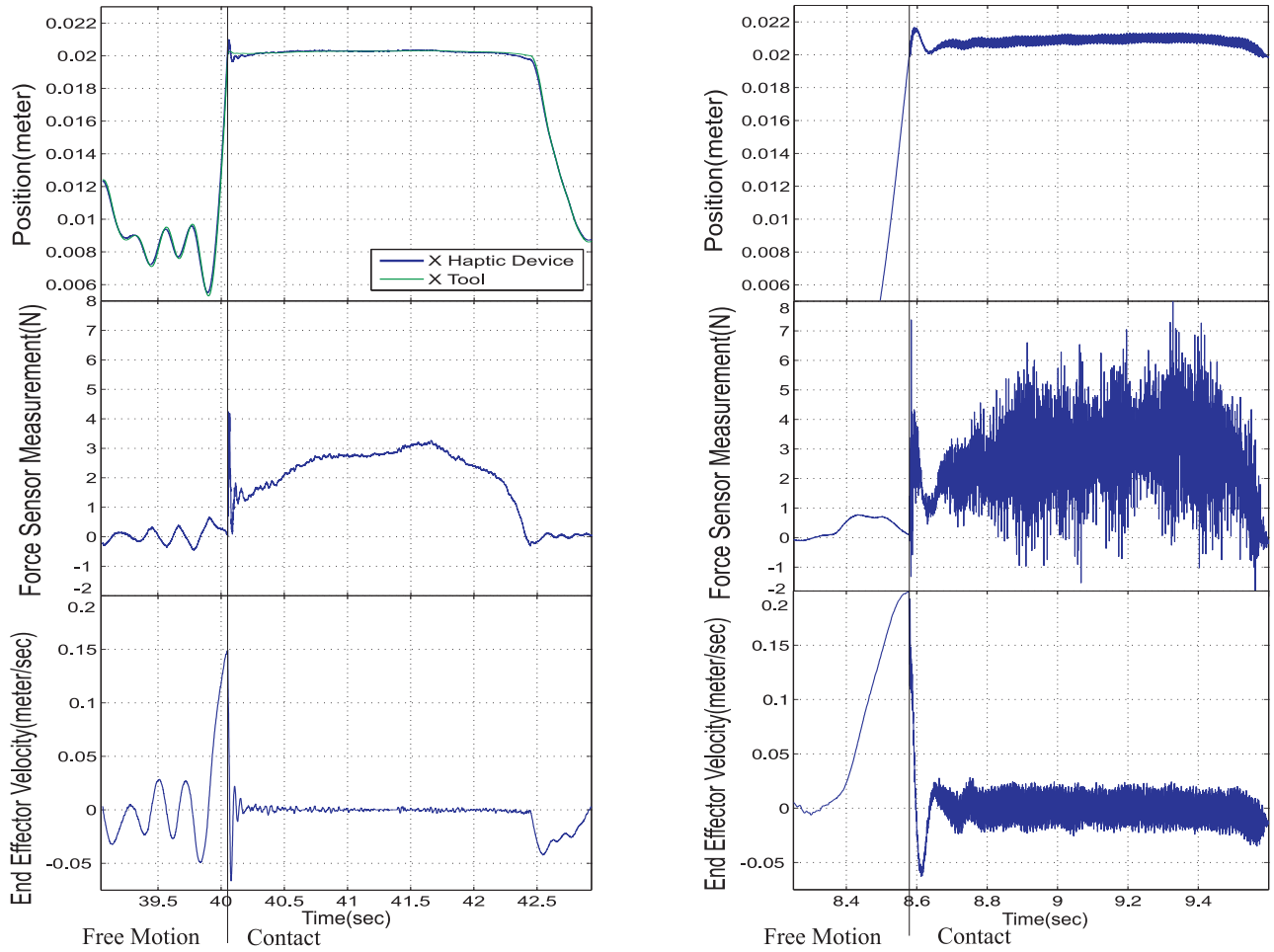

Figure 5: Comparison between the conventional spring-damper coupling and the adaptive controller with admittance-type environment; wall is at $0.02m$; Left: adaptive controller with admittance-type rigid wall in Case 1; $k_{wall} = 10000\frac{N}{m}$, $b_{wall} = 300\frac{Ns}{m}$; Right: conventional virtual coupler; $k_{wall} = 4000\frac{N}{m}$, $b_{wall} = 40\frac{Ns}{m}$.

5.1.2 Contact

Three different types of contact have been implemented.

Case 1: Spring-damper rigid wall

In this case, using a spring-damper model, the wall deflection is calculated based on the measured hand force and the dynamics of the intervening tool. The virtual tool which makes contact with the spring-damper wall is coupled with the haptic device by means of the proposed adaptive controller. In the experiments, the stiffness of the wall could be increased to large values, e.g. $16,000$N/m, and no instability was observed. Nonetheless, increasing the stiffness beyond certain limits did not improve the perception of rigidness as this is effectively determined by the strength of adaptive coupling controller consisting of a feedforward and a feedback term. The use of the feedforward term in the control significantly enhances position tracking between the device and the virtual environment without the need for a large feedback gain that could negatively affect the stability due to discretization.

In the experiments, the performance of the proposed controller for simulating rigid contacts in admittance-type environments is compared with that of a conventional impedance-type spring-damper model and the responses are illustrated in Fig. 5. The proposed adaptive controller is clearly superior as it can stably render contacts with very high stiffnesses. In contrast, the conventional spring-damper coupler exhibits an unstable behavior for much softer walls. There was also a significant difference in the user's perception of rigidness under the two methods.(see also Fig. 6)

Case 2: Constraint-based rigid wall

The proposed controller for admittance-type environment also lends itself to a new constraint-based implementation of rigid contacts. In this approach, upon the initial contact of the tool with the wall, the controller attempts to force the haptic device velocity along the normal direction of the contact surface to zero over a limited number of sample times by stopping the virtual tool over that period. At each sample time the acceleration needed to stop the tool is calculated based on its current velocity and the number of samples left in the stopping period. The tool position x_e, velocity $\dot{x}_e$ and acceleration $\ddot{x}_e$ are passed to the adaptive controller and are used in the calculation of $\dot{x}_r$ and $\ddot{x}_r$ in (11). These values are used in the feedforward term of the control action in (8) resulting in the impulsive forces applied to the user. After the velocity of the tool reaches zero or the stopping period elapses, the velocity and acceleration of the virtual tool are set to zero. For the rest of the contact period $x_e = x_0$, and $\ddot{x}_e = \dot{x}_e = 0$, where x_0 is the tool stopping position. It should be noted that the stoppage phase of the proposed contact model is rather similar to the open-loop force

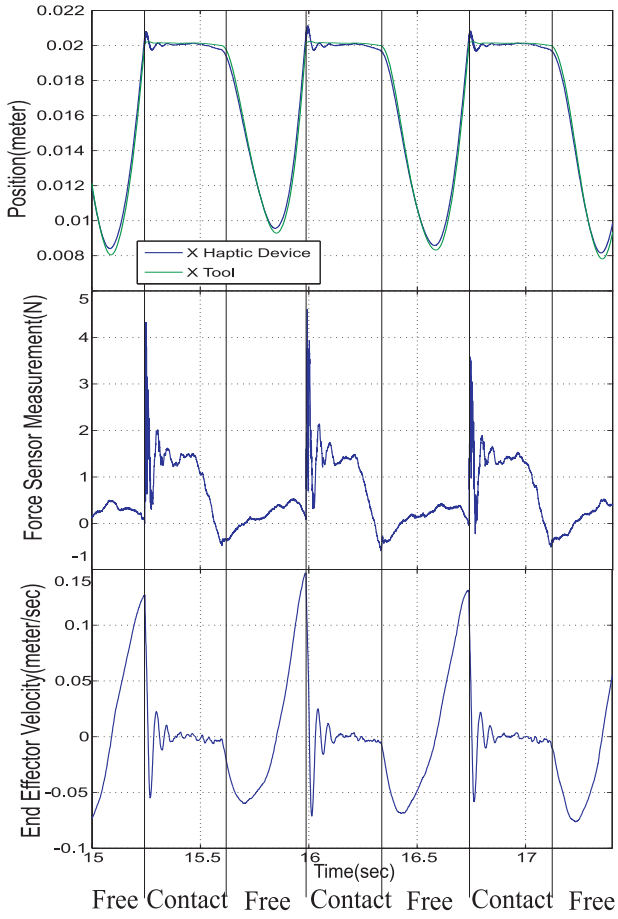

Figure 6: Contact simulation with adaptive controller and admittance-type rigid wall in Case 1; wall is at $0.02m$; Tapping on the wall surface.

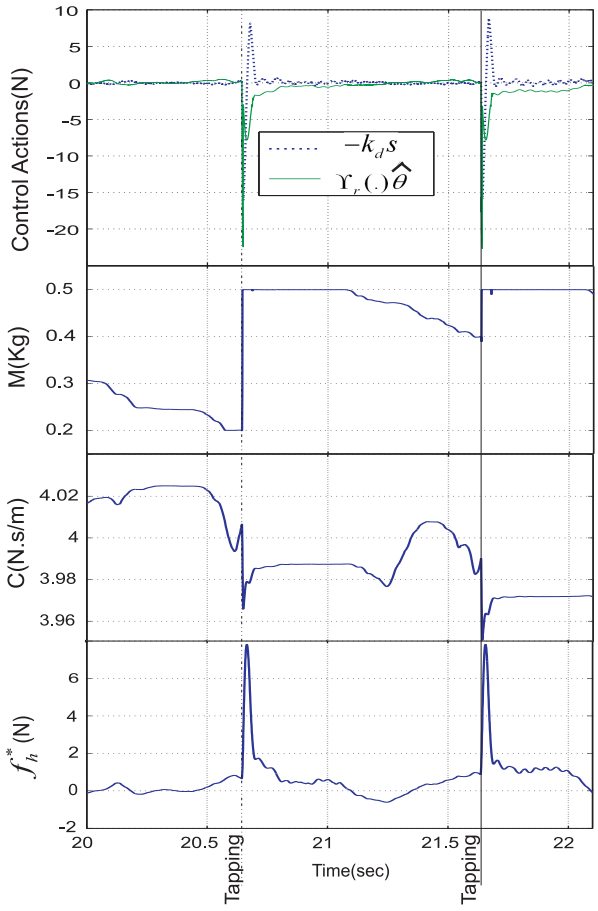

Figure 7: Adaptive controller with admittance-type environment, tapping on the wall, Case 2; Top: feedback and feedforward components of control action; Bottom: estimated parameters, combined mass M, combined damping C, user exogenous force f_h^*.

generation models proposed in [11, 19] among others. However, by having access to the estimated value of the lumped user/device mass, the method in this paper automatically scales the impulsive forces. Furthermore after the initial contact, the proposed approach uses a constraint-based model rather than spring-damper coupling resulting in an enhanced perception of rigidity.

The control action and parameter adaptation are illustrated in Fig. 7. The responses of the adaptive controller with the constraint-based rigid wall are illustrated in Fig. 8. The controller demonstrates an excellent response both in free motion and in rigid contact. In fact, the feeling of rigid contact in this case is even superior to that of the adaptive controller with spring-damper wall.

Case 3: Contact with double mass-spring-damper

In this case, the virtual environment is a double mass-spring-damper shown in Fig. 9 to model contacts with high-order environment dynamics. A completely plastic contact occurs between the virtual tool and the first mass M_1. Upon the detection of initial contact, the system enters a state in which the final velocity of the tool and the mass M_1 based on a plastic contact is calculated. During a predefined number of sample times, similar to the method in Case 2, the desired tool acceleration is generated and used in the adaptive controller. The results of the experiment are displayed in Fig. 10.

5.2 Impedance-type Virtual Environment Simulation

The adaptive control algorithm in Section 3.2 for interacting with impedance-type environments has been implemented. The environment is modeled by an impedance-type spring-damper wall. The system and control parameters are given in Table1. During the experiments, it was discovered that this type of control architecture suffers from similar stability problems as those observed in conventional spring-damper coupling. This may not be surprising as the two approaches use similar mechanisms to generate the environment reaction force. Consequently, the only advantage of this controller over the conventional virtual coupler is in its ability to alter the perceived impedance of the haptic device. The experimental results are given in Fig. 11.

6 Conclusions and Future Work

Adaptive nonlinear control schemes for the haptic interaction of an impedance-type device with impedance and admittance-type virtual environments were proposed. The controllers accommodate an uncertain nonlinear model of the haptic interface and an uncertain mass-spring-damper model of the user. Using measurements of the user force and position/velocity, the controllers can alter the inherent dynamics of the haptic device making them suitable for the use with high-force large-inertia interfaces. The performance and stability of haptic simulation under the proposed methods were analyzed using a Lyapunov-based approach. Rigid con-

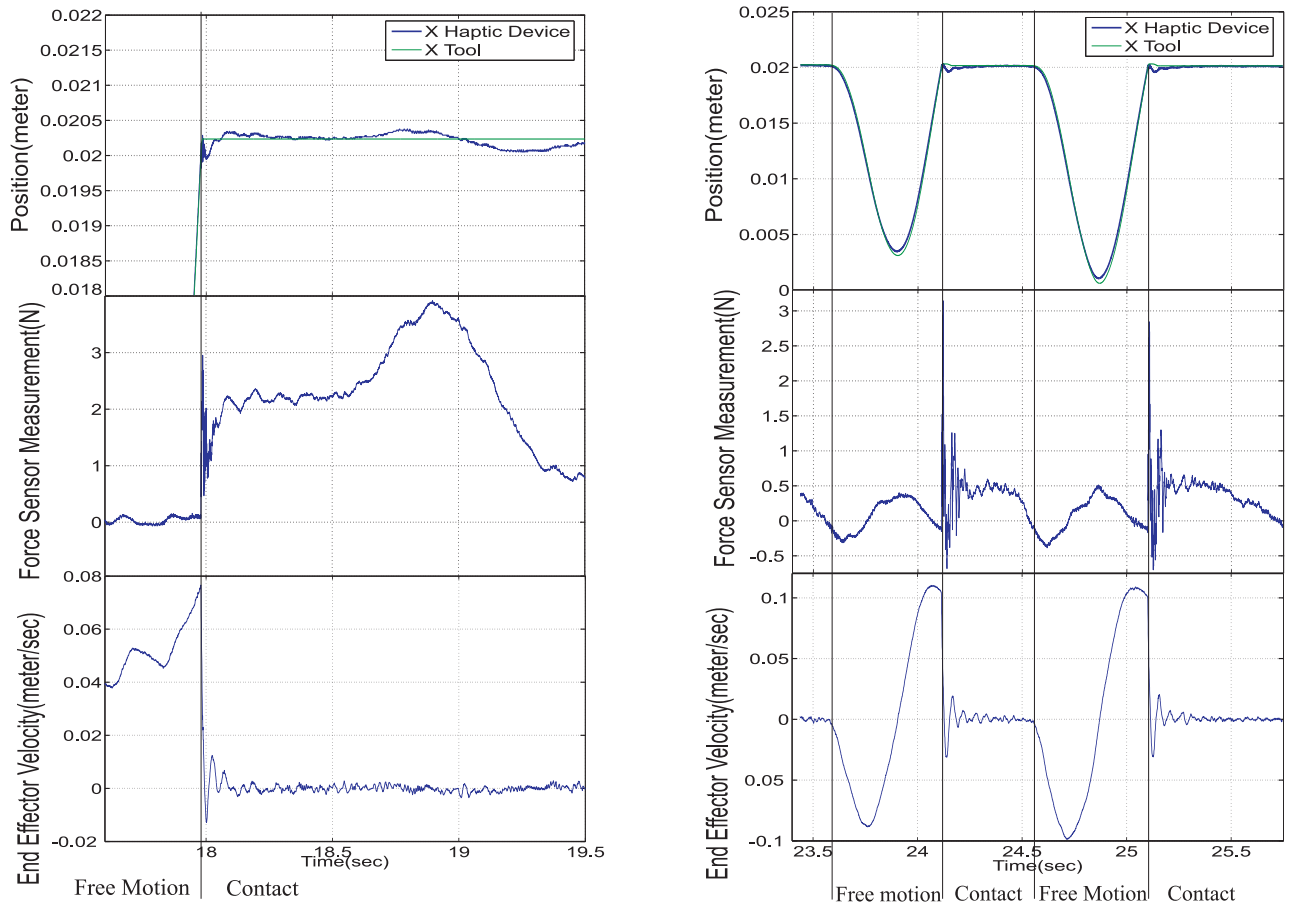

Figure 8: Contact simulation with adaptive controller and admittance-type rigid wall in Case 2; wall is at $0.02m$; Left: sliding on the wall surface; Right: tapping on the wall surface.

tact in admittance-type environments was modeled both as a conventional spring-damper, and as a rigid constraint on the position, velocity and acceleration of the device.

Experiments were conducted to investigate the effectiveness of the proposed controllers. The results demonstrated that the adaptive controller with an admittance-type virtual environment and the constraint-based wall model has by far the best performance in terms of rendering rigid contacts whereas the free motion performance is fairly uniform among all the controllers. The performance of the adaptive controller with impedance-type virtual environment was comparable to that of a conventional virtual-coupler controller. In summary, it can be concluded that the adaptive controller with admittance-type virtual environment is capable of stable rendering of low impedance in free motion and high impedance in rigid contacts making it suitable for high performance haptics applications.

In future, an analytical lower bound for the synthesized impedance of the haptic device in a discrete-time implementation of the proposed controllers will be obtained.

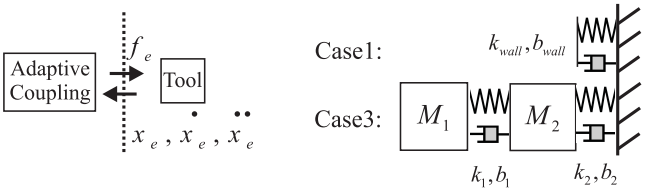

Figure 9: Admittance-type Virtual Environment, Case 1 and 3.

REFERENCES

[1] J. J. Abbott and A. M. Okamura. Effects of position quantization and sampling rate on virtual-wall passivity. *IEEE Transactions on Robotics[see also IEEE Transactions on Robotics and Automation]*, 21(5):952–964, Oct. 2005.

[2] R. J. Adams and B. Hannaford. Control law design for haptic interfaces to virtual reality. *IEEE Transactions on Control Systems Technology*, 10(1):3–13, Jan. 2002.

[3] K. R. Boff and J. E. Lincoln. Engineering data compendium: Human perception and performance. *Armstrong Aerospace Research Laboratory, Wright-Patterson AFB*, 3:166–191, 1988.

[4] C. R. Carignan and K. R. Cleary. Closed-loop control for haptic simulation of virtual environments. *Haptics-e, The Electronic Journal of Haptics Research (http://www.haptics-e.org)*, 2(2):1–14, Feb. 2000.

[5] J. E. Colgate and J. M. Brown. Factors affecting the z-width of a haptic display. In *IEEE Int. Conf. Robotics and Automation, San Diego, CA*, pages 3205–10, 1994.

[6] J. E. Colgate and G. G. Schenkel. Passivity of a class of sampled-data systems: Application to haptic interfaces. *Journal of Robotic Systems.*, 14(1):37–47, Jan. 1997.

[7] J. E. Colgate, M. C. Stanley, and J. M. Brown. Issues in the haptic display of tool use. In *IEEE/RSJ International Conference on Intelligent Robots and Systems, Pittsburgh, PA*, pages 140–145, 1995.

[8] N. Diolaiti, G. Niemeyer, F. Barbagli, and J. K. Salisbury. Stability of haptic rendering: Discretization, quantization, time delay, and

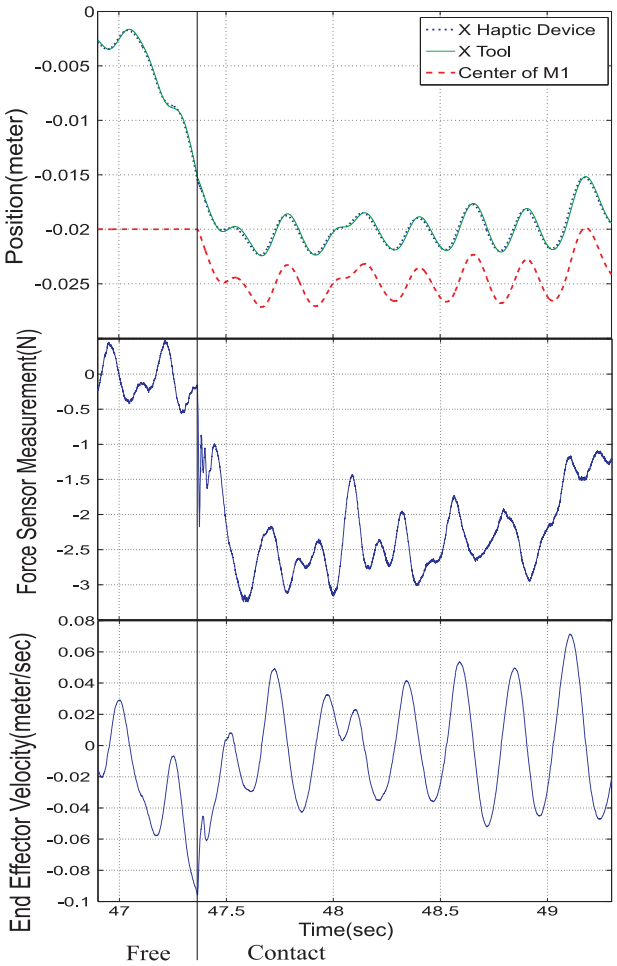

Figure 10: Contact simulation with adaptive controller and admittance-type environment, Case 3.

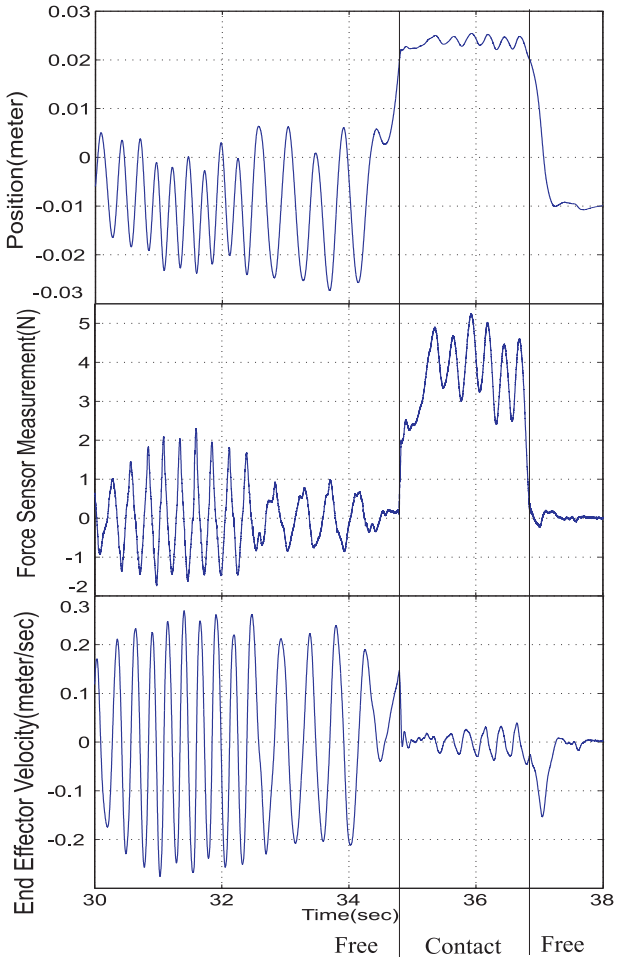

Figure 11: Adaptive control with impedance-type virtual environment; Dynamics of haptic Device are replaced with a $0.25Kg$ mass; $k_{wall} = 1000\frac{N}{m}$, $b_wall = 20\frac{Ns}{m}$.

coulomb effects. *IEEE Transactions on Robotics*, 22(2):256–268, Apr. 2006.

[9] N. Diolaiti, G. Niemeyer, and N. A. Tanner. Wave haptics: Building stiff controllers from the natural motor dynamics. *The International Journal of Robotics Research*, 26(1):5–21, Jan. 2007.

[10] E. L. Faulring, J. E. Colgate, and M. A. Peshkin. The cobotic hand controller: Design, control and performance of a novel haptic display. *The International Journal of Robotics Research*, 25(11):1099–1119, Nov. 2006.

[11] J. P. Fiene and K. J. Kuchenbecker. Shaping event-based haptic transients via an improved understanding of real contact dynamics. *2nd Joint EuroHaptics Conference and Symposium on Haptic Interfaces for Virtual Environment and Teleoperator Systems*, 22(24):170–175, Mar. 2007.

[12] J. J. Gil. and E. Sánchez. Control algorithms for haptic interaction and modifying the dynamical behavior of the interface. In *Proceedings of ENACTIVE05. 2nd International Conference on Enactive Interfaces Genoa, Italy*, Nov. 2005.

[13] A. Gosline and V. Hayward. Time-domain passivity control of haptic interfaces with tunable damping hardware. *Second Joint EuroHaptics Conference and Symposium on Haptic Interfaces for Virtual Environment and Teleoperator System*, pages 164–179, Mar. 2007.

[14] B. Hannaford and J. H. Ryu. Time-domain passivity control of haptic interfaces. *IEEE Transactions on Robotics and Automation*, 18(1):1–10, Feb. 2002.

[15] N. Hogan. Impedance control: An approach to manipulation, part i - theory, part ii - implementation,part iii - applications. *Journal of dynamic systems, measurement, and control*, 107(1):1–7, Mar. 1985.

[16] J. D. Hwang, M. D. Williams, and G. Niemeyer. Toward event-based haptics: Rendering contact using open-loop force pulses. In *The 12th International Symposium on Haptic Interfaces for Virtual Environment and Teleoperator Systems*, pages 24–31, 2004.

[17] F. L. Lewis, D. M. Dawson, and C. Abdallah. *Control of Robot Manipulators*. Prentice Hall PTR Upper Saddle River, NJ, USA, 1993.

[18] P. Malysz and S. Sirouspour. Generalized force/position mappings in bilateral teleoperation with application to enhanced stiffness discrimination(submitted). *IEEE Transactions on Robotics*, 2007.

[19] S. E. Salcudean and T. D. Vlaar. On the emulation of stiff walls and static friction with a magnetically levitated input/output device. *ASME ,Journal of dynamic systems, measurement, and control*, 119(1):127–132, Nov. 1997.

[20] J. J. E. Slotine and W. Li. *Applied Nonlinear Control*. Prentice Hall Englewood Cliffs, New Jersey, 1991.

[21] M. Ueberle and M. Buss. Control of kinesthetic haptic interfaces. In *Proc. IEEE/RSJ Int. Conf. on Intellig. Rob. and Syst., Workshop on Touch and Haptics*, 2004.

[22] W. H. Zhu and S. E. Salcudean. Stability guaranteed teleoperation: An adaptive motion/force control approach. *IEEE Trans. Autom. Control,*, 45(11):1951–1969, Nov. 2000.

[23] C. B. Zilles and J. K. Salisbury. A constraint-based god-object method for haptic display. In *IEEE/RSJ Int. Conf. on Intelligent Robots and Systems, Pittsburgh, PA*, pages 146–151, 1995.